SIMULATIONS OF PHOSPHORYL TRANSFER REACTIONS USING MULTI-SCALE QUANTUM MODELS

Brent A. Gregersen[1], Timothy J. Giese[1], Yun Liu[1], Evelyn Mayaan[1], Kwangho Nam[1], Kevin Range[1], and Darrin M. York[1,*]

[1]Department of Chemistry, University of Minnesota, 207 Pleasant St. SE, Minneapolis, MN 55455–0431
*york@chem.umn.edu

1 INTRODUCTION

Computer simulation provides a tool of enormous potential impact in problems of biocatalysis.[1] From a theoretical perspective, ribozymes present several features that make them more difficult to model relative to most proteins. RNA is inherently highly charged and interacts strongly with monovalent and divalent metal ions and solvent. Careful treatment of long-range electrostatics is critical, as is the inclusion and equilibration of a sufficiently extensive solvation and ion atmosphere. The importance of quantum many-body effects such as polarization and charge transfer, which are neglected in conventional molecular mechanical force fields, is amplified in RNA simulations. Reactions catalyzed by RNA can exhibit fairly large scale conformational changes, such as those encountered in the hammerhead ribozyme, that either precede or occur in concert with reactive chemical steps. The chemistry of many RNA-catalyzed reactions, such as transphosphorylation and phosphate hydrolysis, involves ionic interactions, large polarization effects and transitions between tri-, tetra- and pentavalent phosphorus that require an accurate d-orbital quantum model for a proper description. Reliable molecular simulations of phosphoryl transfer reactions, therefore, need to take into account accurate quantum models, complex macromolecular, ionic and solvent environments, and extensive conformational sampling. Consequently, making accurate predictions about the mechanism and rates of phosphoryl transfer reactions requires theoretical methods that are robust and reliable over a broad range of time and length scales.

The present work describes a multi-faceted theoretical approach toward the development of methods that allow simulations of phosphoryl transfer reactions to be performed with increased reliability and predictive capability. The focus is to outline recent progress in the design of new multi-scale quantum models to study phosphoryl transfer reactions in non-enzymatic and enzymatic environments. Here, “multi-scale” implies the integration of a hierarchy of methods that simultaneously span a broad range of spatial and temporal domains and work in concert to provide insight into complex problems.

2 METHODS

The present work describes an approach toward the design of multi-scale quantum models for phosphoryl transfer reactions. In this section, a brief overview is given of some of the general theoretical methods and computational details

2.1 Density-functional calculations

Density-functional calculations, unless otherwise stated, were performed using the B3LYP exchange-correlation functional[2, 3] with the 6–31++G(d,p) basis set for geometry and frequency calculations followed by single-point energy refinement with the 6–311++G(3df,2p) basis set in a manner analogous to recent studies of biological phosphates.[4–7] Energy minimum and transition state geometry optimizations were performed in redundant internal coordinates with default convergence criteria,[8] and stability conditions of the restricted closed shell Kohn-Sham determinant for each final structure were verified.[9, 10] Frequency calculations were performed to establish the nature of all stationary points and to allow evaluation of thermodynamic quantities. Solvent was treated using the PCM solvation model.[11, 12] Due to instabilities in the geometry optimization of the DFT calculations on the solvated potential energy surface, solvent corrections were taken into account by single point calculations at the gas phase-optimized B3LYP/6–31++G(d,p) geometries, as in previous work.[4–7] All density-functional calculations, unless otherwise stated, were performed with the GAUSSIAN03[13] suite of programs.

2.2 Semiempirical calculations

All semiempirical/implicit solvation calculations were performed using a modified version of the MNDO97 program,[14] and often employ the combined MNDO/d Hamiltonian[15] and smooth COSMO method.[16] Details of the method, implementation and testing have been presented elsewhere.[17, 18] Convergence criteria for the SCF energy was 10^{-6} eV, and for geometry optimizations was 1.0 kcal/mol/Å on the gradient norm. Unless otherwise stated, solvation calculations used a discretization level of 110 points per sphere, smooth COSMO switching parameter $_s \approx 1.0$, and shift parameter 0.5 as described in detail elsewhere.[17] The MNDO/d and smooth COSMO methods have been implemented into the MNDO97 code[14] and interfaced to the CHARMM molecular modeling package[19] and will be available in future MNDO and CHARMM releases.

2.3 Hybrid QM/MM calculations

Hybrid QM/MM calculations were performed using the MNDO97 program[14] interfaced with CHARMM.[19] Activated dynamics calculations were performed using either stochastic boundary molecular dynamics (SBMD)[20, 21] without cut-off, or else full cubic periodic boundary conditions using a recently introduced linear-scaling QM/MM-Ewald method[22] that employs the smooth particle mesh Ewald (PME) method.[23, 24] Unless otherwise stated, simulations were performed at constant temperature (298.15 K) with a 0.5 fs integration time step, and used the TIP3P water model[25] with SHAKE constraints[26] on the internal water geometries. Potential of mean force (PMF) profiles were determined using umbrella sampling[27] and the weighted histogram analysis method (WHAM).[28]

3 RESULTS AND DISCUSSION

3.1 Density-functional calculations of phosphoryl transfer reactions

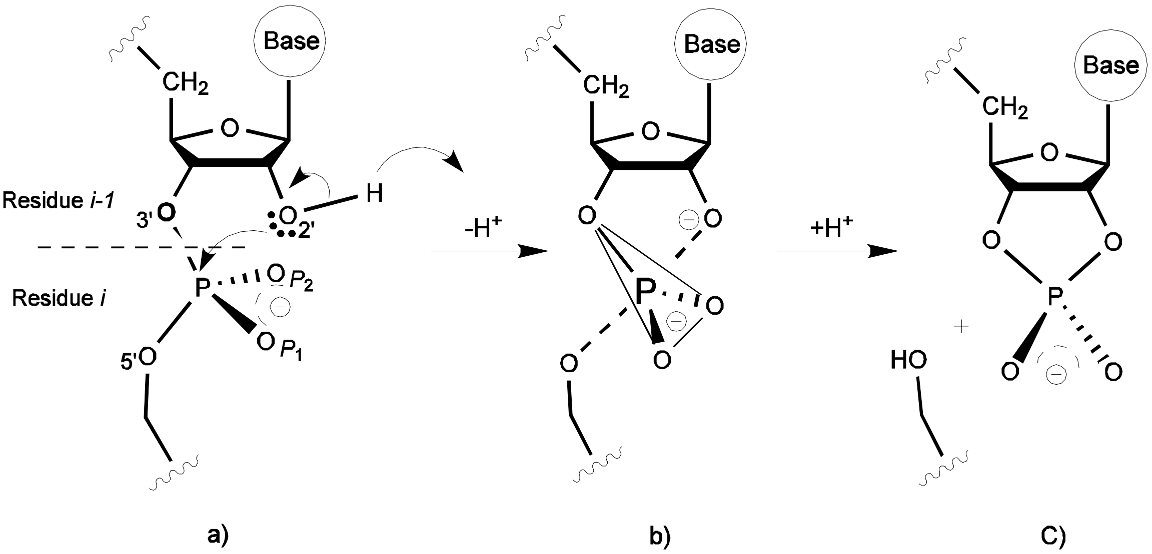

Scheme 1 *RNA transesterification*

As an illustrative example of a model phosphoryl transfer reaction, consider the cleavage transesterification reaction (Scheme 1) that occurs in RNA, and is catalyzed by the prototype RNA enzymes such as the hammerhead[29, 30] and hairpin[31, 32] ribozymes. One method to probe the mechanism of ribozymes is to introduce chemical modifications at specific sites,[33–38] and make mechanistic inferences from the measured change in reaction rate. A commonly applied modification involves the substitution of key phosphoryl oxygens with sulfur.[33, 35, 38–40] A subsequent change in the reaction rate is called a thio effect, and can provide insight into the specific role these positions play in the biological reaction. However, it is often the case that multiple mechanistic pathways are able to fit the observed kinetics equally well.[41] Theoretical methods offer a potentially powerful tool to aid in the mechanistic interpretation of experimental kinetic data and provide additional atomic-level insight into the structural and chemical reaction dynamics.[1, 42–44]

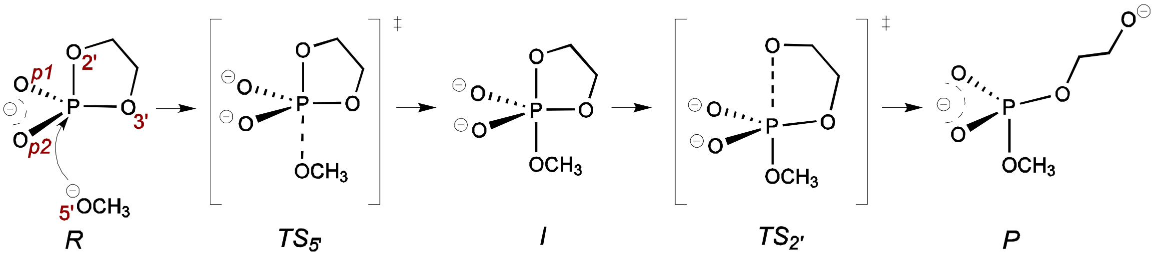

Scheme 2 *In-line dianionic mechanism of ethylene phosphate methanolysis (a reverse-reaction model for RNA phosphate transesterification)*

Consider the dianionic in-line mechanism of methanolysis of ethylene phosphate (Scheme 2) as reverse reaction model for RNA transesterification. Table 1 lists the forward/reverse rate-controlling free energy barriers for dianionic methanolysis/transesterification reactions in the gas phase and in solution. The focus here is to highlight key results for the solution barriers, a full discussion of both gas-phase and solution data are provided elsewhere.[45] Solvent has a tremendous stabilization effect for all the dianionic reactions. In general, sulfur substitution tends to yield lower solvation free energies, due to the larger size and more delocalized concentration of negative charge of sulfur.

Table 1 *Forward and reverse rate-controlling free energy barriers for dianionic methanolysis reactions in the gas phase and in solution*[a]

	$\Delta G^{\ddagger}$		$\Delta G^{\ddagger}_{aq}$					
			PCM		CPCM		SM5	
Reaction	Fwd	Rev	Fwd	Rev	Fwd	Rev	Fwd	Rev
native	98.3 (0.0)	41.7 (0.0)	41.1 (0.0)	28.3 (0.0)	40.0 (0.0)	26.1 (0.0)	30.2 (0.0)	23.1 (0.0)
S: O_{P1}	93.0 (-5.3)	39.0 (-2.7)	40.6 (-0.5)	26.7 (-1.6)	39.0 (-1.0)	24.2 (-1.9)	27.7 (-2.5)	20.0 (-3.1)
S: O_{P1},O_{P2}	90.3 (-8.0)	38.1 (-3.6)	41.6 (0.5)	27.5 (-0.8)	39.8 (-0.2)	24.4 (-1.7)	27.9 (-2.3)	18.9 (-4.2)
S: $O_{3'}$	89.4 (-8.9)	35.9 (-5.8)	36.3 (-4.8)	23.4 (-4.9)	36.7 (-3.3)	22.4 (-3.7)	25.4 (-4.8)	19.7 (-3.4)
S: $O_{2'}$	88.0 (-10.3)	62.6 (20.9)	42.4 (1.3)	51.2 (22.9)	41.7 (1.7)	48.8 (22.7)	27.7 (-2.5)	49.4 (26.3)
S: $O_{5'}$	108.0 (9.7)	25.1 (-16.6)	55.9 (14.8)	21.8 (-6.5)	53.8 (13.8)	19.9 (-6.2)	51.5 (21.3)	15.1 (-8.0)

[a] Relative free energy values (kcal/mol) in the gas phase ($G^{\ddagger}$) and in solution ($G^{\ddagger}_{aq}$) for the rate-controlling transition state of the forward (Fwd) dianionic methanolysis reaction (i.e., relative to the reactants at infinite separation), and of the reverse (Rev) dianionic transesterification reaction (i.e., relative to the product state). Shown in parentheses are the relative free energy differences ($G^{\ddagger}$ and $G^{\ddagger}_{aq}$) with respect to the native reaction.

Overall, in aqueous solution for both forward (methanolysis) and reverse (transesterification) reactions, only moderate rate changes with thio substitution are predicted at the non-bridging phosphoryl oxygen positions. This result is consistent with experimental results for RNA analogs with non-bridging thio substitutions that exhibit only modest thio effects.[46–48] Substitution at the bridging $O_{3'}$ position leads to a decrease in the activation barrier by 3.3–4.8 kcal/mol. This is consistent with the experimentally observed 200-fold[49] and 2000-fold[50] rate enhancements observed for base-catalyzed hydrolysis of 3´-thio modified RNA dinucleotides. Thio substitution at the $O_{2'}$ position has a moderate effect on the forward methanolysis activation barrier, and also a considerable increase in the reverse transesterification barrier that ranges from 22.7–26.3 kcal/mol. This is consistent with kinetic measurements for modified 2´-thio ribonucleotides[51] that indicate thiolate attack to the phosphate center is 107 times slower than the corresponding alkoxide. Thio substitution at the $O_{5'}$ position results in the largest forward activation barrier (51.5–55.9 kcal/mol). These results are consistent with the increased stability of the 5′ thiolate leaving group as indicated by lower theoretical and experimental pKa values of thiols with respect to the corresponding alcohols,[52, 53] and by the experimentally observed increase in rate constants for transphosphorylation with enhanced leaving groups.[39, 54–56]

The application highlighted above represents one example of the use of DFT methods to elucidate key factors that influence reactivity in phosphoryl transfer reactions. In order to perform simulations of phosphoryl transfer reactions with multi-scale quantum models, many such DFT calculations need to be performed in order to create the data necessary to design new semiempirical Hamiltonian models for use in hybrid QM/MM simulations. Toward this end, a large database of Quantum Calculations for RNA catalysis, QCRNA, has been constructed. The database currently contains over 1,700 molecular structures and complexes and 200 chemical mechanisms relevant to phosphoryl transfer, and has recently been made available on-line at http://riesling.chem.umn.edu/QCRNA.

3.2 Hybrid QM/MM simulations of phosphoryl transfer reactions

A particularly useful strategy to study chemical reactions in complex aqueous biological environments is to perform activated molecular dynamics simulations with hybrid QM/MM potentials[57–60] to derive reaction free energy profiles for different possible mechanistic pathways. A key factor in these simulations is to employ quantum methods that are sufficiently accurate and efficient to derive reliable free energy results.

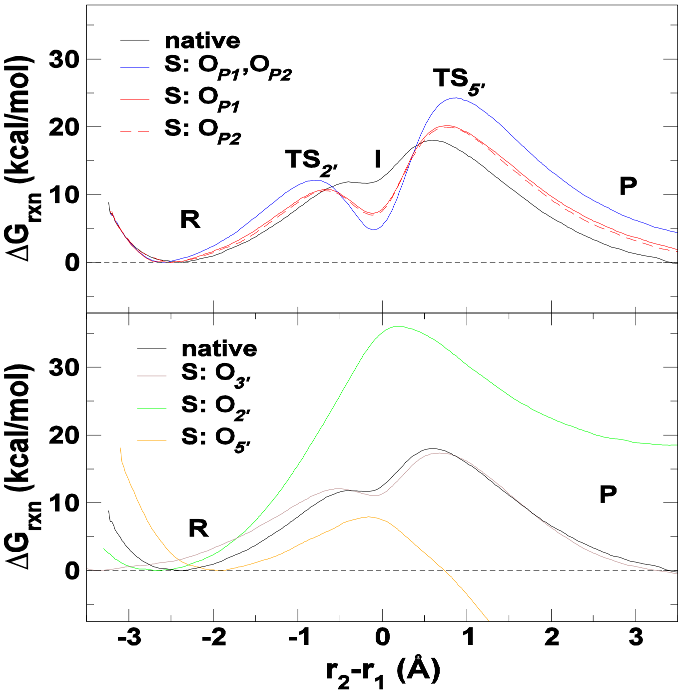

Figure 1 *Free energy profiles for native and thio-substituted dianionic transesterification reactions.*

Figure 1 shows the free energy profiles for the native (unsubstituted) and sulfur-substituted in-line dianionic attack mechanism of transesterification. The trends observed are qualitatively similar to those derived from DFT with implicit solvation discussed in the previous section. A detailed discussion of the QM/MM profiles, average geometric parameters and relative free energy values has been presented elsewhere.[61] The focus here is to highlight the role of explicit solvation on the mechanism and barriers.

Solvation plays a key role in stabilizing the dianionic reactive intermediates. Figure 2 illustrates the change that occurs in the radial distribution function of water oxygens around the nucleophilic (2´) and leaving group (5´) positions as the reaction proceeds. In the transesterification reaction, as the activated 2´ nucleophile approaches phosphorus in the endocyclic bond formation step, it must become partially de-solvated. The barrier to de-solvation raises the free energy for $TS_{2'}$ more for the doubly thio-substituted reaction than the native reaction due to the larger size of the non-bridging sulfur atoms. In the rate-controlling exocyclic cleavage step, the 5´ leaving group becomes solvated as the reaction proceeds as indicated by the appearance of an ordered solvation shell in Fig. 4. Hence, the thio substitution exhibits electronic effects as well as solvation effects, each of which is sensitive to the position of the thio substitution. For thio substitution at the non-bridging position, the solvation effect appears dominant, whereas at the bridging nucleophilic and leaving group positions, the electronic effects have the greatest influence.

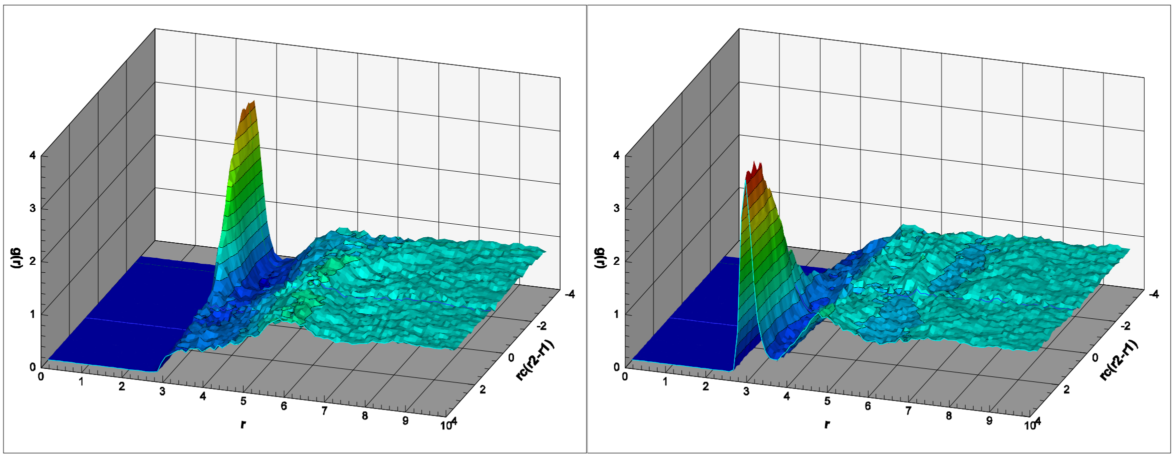

Figure 2 *Radial distribution functions of water oxygens (O_w) around the O2´ nucleophile (left) and O5´ leaving group (right) as a function of reaction coordinate (reactant state is in the background, product state is in the foreground) for the doubly thio-substituted reaction.*

3.3 Smooth implicit solvation models

There is growing interest in the development of implicit solvation models that can be used simultaneously with molecular simulation and linear-scaling electronic structure methods to address complicated biological problems. Certain solvation methods, particularly those of the "boundary element" type,[62] are among the most widely applied in electronic structure calculations.[11, 63] Incorporated into electronic structure or molecular mechanics methods, implicit solvation models provide a powerful tool to study solution-phase molecular properties, chemical reactions, and molecular dynamics. Consequently, it is important to ascertain the reliability of new and existing quantum and solvation models in order to design improved multi-scale quantum models for these reactions.

Recently, a smooth COSMO model[16] has been introduced that circumvents many of the problems encountered by conventional boundary-element methods through the use of Gaussian functions for expansion of the reaction field surface charges and a differentiable switching layer that allows new surface elements to appear and disappear smoothly with respect to the energy. The method has been implemented with analytic gradients[17] within a d-orbital semiempirical framework[15, 64] and applied to phosphoryl transfer reactions.[18]

Figure 3 compares PMF profiles derived from QM/MM simulation and from the MNDO/d-smooth COSMO (MNDO/d- SCOSMO) method for the transesterification of 3´-ribose, 5´-methyl phosphodiester and the doubly thio-substituted derivative. The two methods agree well for both profiles, each predicting similar transition states and intermediates. The MNDO/d- SCOSMO requires a fraction of the computational cost of the explicit QM/MM simulation. One of the key results that arise from this comparison is that the use of the present MNDO/d-SCOSMO model may afford an avenue for efficient parameterization of QM/MM van der Waals radii that are key to obtain reliable free energy profiles of reactions that involve ionic species.[65] A large number of radii can be examined rapidly using the MNDO/d-SCOSMO model, and the most promising sets of radii can then be applied in the more expensive QM/MM simulations.

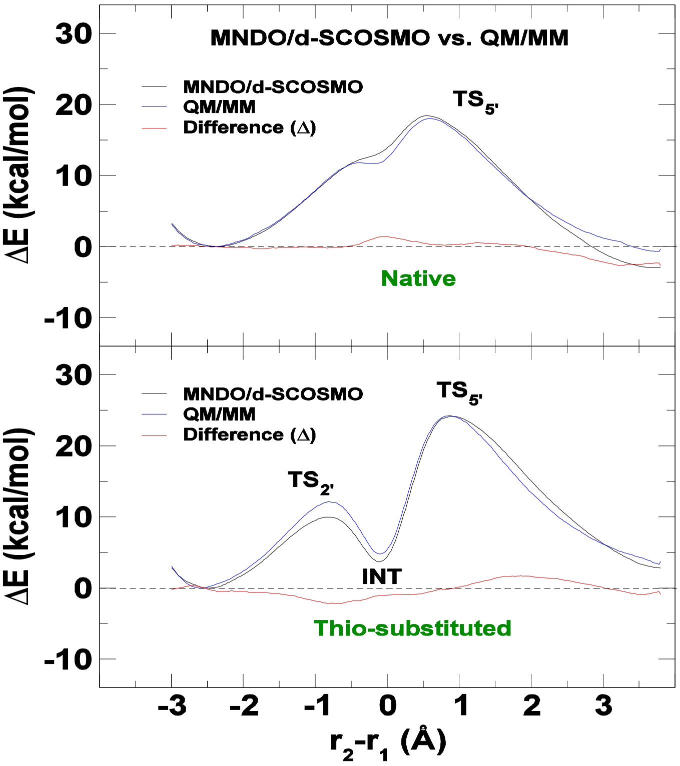

Figure 3 *MNDO/d-SCOSMO and QM/MM reaction profiles of the transesterification of 3´-ribose, 5´-methyl phosphodiester in the native (top) and doubly sulfur-substituted (bottom) forms. The reaction coordinate is defined to be* $r_2 - r_1$*. Shown are the relaxed solution-phase energy profiles optimized with MNDO/d-SCOSMO (black), the potential of mean force profile obtained from hybrid QM/MM simulation in explicit solvent (blue), and*

the difference between the two curves (red). All energies (kcal/mol) are with respect to the reactant.

3.4 Linear-scaling electrostatic and solvation methods

3.4.1 Linear-scaling Ewald method for hybrid QM/MM calculations

In hybrid QM/MM potential models, the electrostatic environment affects the quantum electronic polarization of the solute[66] and plays a significant role in the stabilization of macromolecules in solution[67] and the rate enhancement of some enzymes.[68] Consequently, it is critical to compute long-range electrostatic interactions accurately in QM/MM simulations of biochemical reactions. Nonetheless, due to the lack of availability of algorithms that extend linear-scaling electrostatic methods to hybrid QM/MM potentials, a large percentage of QM/MM applications routinely employ electrostatic cut-offs.[69]

The present section highlights a recently developed linear-scaling Ewald method for efficient calculation of long-range electrostatic interactions in hybrid QM/MM simulations using semiempirical quantum models. Details of the method and simulations have been presented elsewhere.[22] To characterize the effects of treatment of long-range electrostatic interactions on QM/MM free energy profiles, the dissociative phosphoryl transfer reaction of acetyl phosphate (Figure 4) was examined using the semiempirical MNDO/d model.[15, 27] Comparisons were made between periodic boundary molecular dynamics (PBMD) simulations using QM/MM-Ewald method and using spherical electrostatic cut-offs.

The effect of cut-off on the PMF profile for the dissociative phosphoryl transfer reaction of acetyl phosphate (Figure 4) is dramatic. The free energy of dissociation from current PMF profiles with QM/MM-Ewald method is 6.8 kcal/mol for acetyl phosphate, and the activation free energy barrier is 12.2 kcal/mol. The effect of cut-off in the PBMD simulations raised the activation free energy barrier to 13.8 kcal/mol (an increase of 1.6 kcal/mol, or 13%). The effect of cut-off for this reaction is to cause an artificial linear drift in the PMF profile at fairly large separation, and raise the activation free energy barrier at short distance. This artifact vanishes when the QM/MM-Ewald method is employed. The cut-off results are comparable to those of Bader and Chandler,[70] in which PMFs of like-charged anions increased with inter-ionic distance, while PMFs using Ewald sum become flat at long range. Despite the known problems associated with the use of electrostatic cut-offs, the majority of present day applications of QM/MM methods routinely employs cut-offs in simulations of biological reaction dynamics.[69] Consequently, the present method offers an important extension of linear-scaling Ewald techniques to hybrid QM/MM calculations of large biological systems.

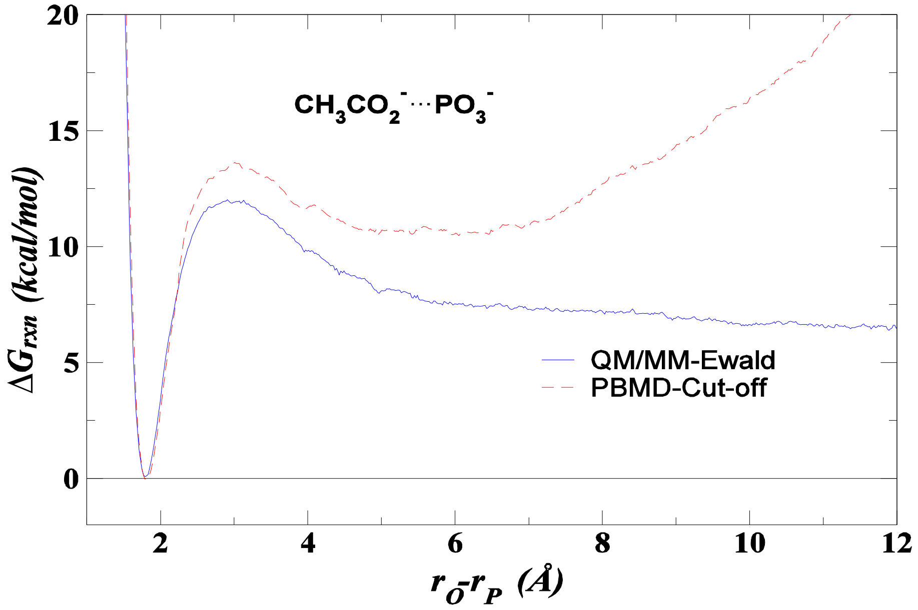

Figure 4 *Free energy profiles from PBMD simulations using hybrid QM/MM-Ewald sum potential (solid blue line) and with 11.5 A cut-off (dashed red line) for the dissociation of acetyl phosphate ($CH3CO^{-2} \cdots PO^{-3}$) in water.*

3.4.2 Variational electrostatic projection method for modeling the solvated macromolecular environment

Recently, a new approach has been introduced to efficiently model a complex solvated macromolecular environment in hybrid QM/MM simulations that does not require explicit consideration of a large simulation cell as is required for Ewald simulations. In this method a variational electrostatic projection (VEP) technique[71] is employed to determine a set of charges on a discretized surface surrounding, for example, a ribozyme active site, such that these charges accurately reproduce the electrostatic potential and forces inside the surface.

In the present section, a new VEP-charge scaling (VEP-cs) method is outlined where charges on a relatively small set of frozen atoms in a SBMD simulation can be re-scaled such that the electrostatic potential and forces inside the active dynamical region reflect the fully solvated macromolecular electrostatic environment. The VEP-charge scaling method has the advantage that the solvent effect due to the entire macromolecular charge distribution is represented, and the method does not require specification of fitting points.

Table 2 compares the average magnitude of the force errors associated with the VEP, VEP-RVM, and VEP-cs methods in the active dynamical region of the hammerhead ribozyme system.[71] In the VEP-charge scaling method, a charge scaling zone of size R_{cs} is employed (Figure 5). Two key quantities regulate the accuracy of the methods: 1) the discretization level (number of points) of the variational projection surface (N), and 2) the discretization level of the intermediate surface used in the RVM and charge scaling procedures (N). Also shown for comparison is a hybrid method that uses the VEP-RVM procedure with an auxiliary set of charge scaling points (VEP-RVM+cs).

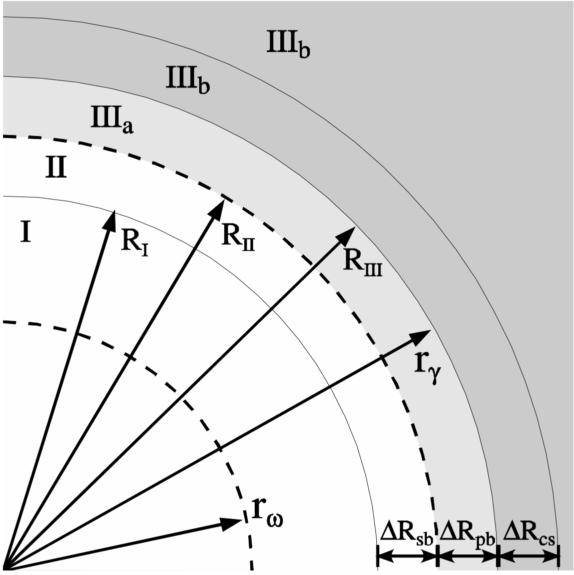

Figure 5 *Regions defined by the VEP charge scaling procedure. Regions I and II are the active dynamical regions, with the atoms of region I propagated using Newtonian dynamics, and those of region II propagated using Langevin dynamics. Region III (subdivided into IIIa and IIIb) comprises the external macromolecular and solvent environment that, in the present work are held fixed. The electrostatic potential due to atoms of external environment (region IIIb), excluding those of the projection buffer (region IIIa), is replaced by the electrostatic potential of auxiliary charges placed at the centers of the atoms in the charge scaling region* R_{cs}. *The surface is used temporarily in the VEP-cs method to derive the scaled charges. An additional surface at r can be used in conjunction with the charge scaling procedure.*

The direct VEP method with R_{cs}=2.0 Å leads to average relative force errors in the active dynamical region of 1.07, 0.30 and 0.056 % for N values of 302, 590 and 1202, respectively. The VEP-RVM method offers considerable improvement, decreasing the relative errors by approximately 2 orders of magnitude, irrespective of the N value. The VEP-cs method slightly outperforms the VEP-RVM method for N discretization levels of 302 and 590 points. With the VEP-RVM+cs method, little improvement is gained with smaller N and N discretization levels, but considerably higher accuracy is obtained with N=5810 and N =1202.

Table 2 *Comparison of relative force errors in the active dynamical region of the hammerhead ribozyme (as described in reference 71) for the VEP-based methods (*R_{II} *= 20.0 Å,* R_{pb} *= 2.0 Å). The charge-scaling region contained a total of 1761 atoms (the ribozyme plus non-solute atoms in the charge-scaling buffer region,* R_{cs} *= 2.0 Å). The atoms in the charge-scaling region were not variationally projected.*

Method	N_ω	Relative RMS Force Error			
		$N_\gamma = 0$	$N_\gamma = 302$	$N_\gamma = 590$	$N_\gamma = 1202$
VEP	–		1.071E-02	2.959E-03	5.558E-04
VEP-RVM	1202		8.665E-04	6.035E-05	1.197E-06
	3890		8.409E-04	5.753E-05	1.200E-06
	5810		8.551E-04	5.779E-05	1.207E-06
VEP-cs	1202	1.408E-05			
	3890	1.446E-06			
	5810	2.157E-06			
VEP-RVM+cs	1202		6.380E-06	9.058E-06	1.270E-06
	3890		6.295E-07	2.902E-07	3.208E-07
	5810		1.032E-06	4.247E-07	7.441E-08

To put these results into perspective, the total hammerhead system with full solvation and counter table consists of over 20,000 atoms. In the case of the VEP-cs method, the interaction of the atoms of the active dynamical region with the 20,000 external frozen atoms is replaced by the interaction with around 2,000 atoms that make up the charge scaling zone. This represents almost an order of magnitude reduction of pairwise interactions with the external environment with a relative force error on the order of 0.001%. Further improvement can be gained using a hybrid VEP-RVM+cs approach where and additional set of N surface elements are used to augment the set of scaled charges in the charge scaling buffer.

4 CONCLUSION

The present work describes the development and application of multi-scale quantum models for simulations of phosphoryl transfer reactions. The approach is multi-faceted, and contains components that include high-level density-functional calculations, semiempirical hybrid QM/MM quantum potentials, smooth implicit solvation models and linear-scaling methods for treatment of electrostatic interactions of the solvated macromolecular environment. These methods work together to provide deeper insight into the mechanisms of phosphoryl transfer reactions in complex environments and processes that simultaneously span a broad range of spatial and temporal domains. It is the hope that further development and application of multi-scale quantum models for phosphoryl transfer reactions may, together with experiment, ultimately unravel important questions in cell signaling, energy transfer and RNA catalysis.

5 ACKNOWLEDGMENT

D.Y. is grateful for financial support provided by the National Institutes of Health (grant GM62248), and the Army High Performance Computing Research Center (AHPCRC) under the auspices of the Department of the Army, Army Research Laboratory (ARL) under Cooperative Agreement number DAAD19-01-2-0014.

References

1 Warshel, A. *Computer Modeling of Chemical Reactions in Enzymes and Solutions*. John Wiley and Sons, New York, **1991**.

2 Becke, A. D. *J. Chem. Phys.* **1993**, *98*, 5648–5652.

3 Lee, C.; Yang, W.; Parr, R. G. *Phys. Rev. B.* **1988**, *37*, 785–789.

4 Range, K.; McGrath, M. J.; Lopez, X.; York, D. M. *J. Am. Chem. Soc.* **2004**, *126*, 1654–1665.

5 López, C. S.; Faza, O. N.; Gregersen, B. A.; Lopez, X.; de Lera, A. R.; York, D. M. *Chem. Phys. Chem.* **2004**, *5*, 1045–1049.

6 Mayaan, E.; Range, K.; York, D. M. *J. Biol. Inorg. Chem.* **2004**, *9*, 807–817.

7 López, C. S.; Faza, O. N.; R. de Lera, A.; York, D. M. *Chem. Eur. J.* **2005**, *11*, 2081–2093.

8 Peng, C.; Ayala, P. Y.; Schlegel, H. B.; Frisch, M. J. *J. Comput. Chem.* **1996**, *17*, 49–56.

9 Bauernschmitt, R.; Ahlrichs, R. *J. Chem. Phys.* **1996**, *104*, 9047–9052.

10 Seeger, R.; Pople, J. A. *J. Chem. Phys.* **1977**, *66*, 3045–3050.

11 Tomasi, J.; Persico, M. *Chem. Rev.* **1994**, *94*, 2027–2094.

12 Cossi, M.; Scalmani, G.; Rega, N.; Barone, V. *J. Chem. Phys.* **2002**, *117*, 43–54.

13 Frisch, M. J.; Trucks, G. W.; Schlegel, H. B.; Scuseria, G. E.; Robb, M. A.; Cheeseman, J. R.; Montgomery Jr., J. A.; Vreven, T.; Kudin, K. N.; Burant, J. C.; Millam, J. M.; Iyengar, S. S.; Tomasi, J.; Barone, V.; Mennucci, B.; Cossi, M.; Scalmani, G.; Rega, N.; Petersson, G. A.; Nakatsuji, H.; Hada, M.; Ehara, M.; Toyota, K.; Fukuda, R.; Hasegawa, J.; Ishida, M.; Nakajima, T.; Honda, Y.; Kitao, O.; Nakai, H.; Klene, M.; Li, X.; Knox, J. E.; Hratchian, H. P.; Cross, J. B.; Adamo, C.; Jaramillo, J.; Gomperts, R.; Stratmann, R. E.; Yazyev, O.; Austin, A. J.; Cammi, R.; Pomelli, C.; Ochterski, J. W.; Ayala, P. Y.; Morokuma, K.; Voth, G. A.; Salvador, P.; Dannenberg, J. J.; Zakrzewski, V. G.; Dapprich, S.; Daniels, A. D.; Strain, M. C.; Farkas, O.; Malick, D. K.; Rabuck, A. D.; Raghavachari, K.; Foresman, J. B.; Ortiz, J. V.; Cui, Q.; Baboul, A. G.; Clifford, S.; Cioslowski, J.; Stefanov, B. B.; Liu, G.; Liashenko, A.; Piskorz, P.; Komaromi, I.; Martin, R. L.; Fox, D. J.; Keith, T.; Al-Laham, M. A.; Peng, C. Y.; Nanayakkara, A.; Challacombe, M.; Gill, P. M. W.; Johnson, B.; Chen, W.; Wong, M. W.; Gonzalez, C.; Pople, J. A. Gaussian, Inc., Pittsburgh PA, 2003.

14 Thiel, W. *Program MNDO97*. University of Zurich, 1998.

15 Thiel, W.; Voityuk, A. A. *J. Phys. Chem.* **1996**, *100*, 616–626.

16 York, D. M.; Karplus, M. *J. Phys. Chem. A* **1999**, *103*, 11060–11079.

17 Khandogin, J.; Gregersen, B. A.; Thiel, W.; York, D. M. *J. Phys. Chem. B* **2005**, *109*, 9799-9809.

18 Gregersen, B. A.; Khandogin, J.; Thiel, W.; York, D. M. *J. Phys. Chem. B* **2005**, *109*, 9810-9817.

19 Brooks, B. R.; Bruccoleri, R. E.; Olafson, B. D.; States, D. J.; Swaminathan, S.; Karplus, M. *J. Comput. Chem.* **1983**, *4*, 187–217.

20 Brooks III, C. L.; Karplus, M. *J. Chem. Phys.* **1983**, *79*, 6312–6325.

21 Brooks III, C. L.; Brunger, A.; Karplus, M. *Biopolymers* **1985**, *24*, 843–865.

22 Nam, K.; Gao, J.; York, D. M. *J. Chem. Theory Comput.* **2005**, *1*, 2–13.

23 Essmann, U.; Perera, L.; Berkowitz, M. L.; Darden, T.; Hsing, L.; Pedersen, L. G. *J. Chem. Phys.* **1995**, *103*, 8577–8593.

24 Sagui, C.; Darden, T. A. *Annu. Rev. Biophys. Biomol. Struct.* **1999**, *28*, 155–179.

25 Jorgensen, W. L.; Chandrasekhar, J.; Madura, J. D.; Impey, R. W.; Klein, M. L. *J. Chem. Phys.* **1983**, *79*, 926–935.

26 Ryckaert, J. P.; Ciccotti, G.; Berendsen, H. J. C. *J. Comput. Phys.* **1977**, *23*, 327–341.

27 Torrie, G. M.; Valleau, J. P. *J. Comput. Phys.* **1977**, *23*, 187–199.

28 Kumar, S.; Bouzida, D.; Swendsen, R.; Kollman, P.; Rosenberg, J. *J. Comput. Chem.* **1992**, *13*, 1011–1021.

29 Scott, W. G.; Murray, J. B.; Arnold, J. R. P.; Stoddard, B. L.; Klug, A. *Science* **1996**, *274*, 2065–2069.

30 Scott, W. G. *Q. Rev. Biophys.* **1999**, *32*, 241–294.

31 Walter, N. G.; Burke, J. M. *Curr. Opin. Chem. Biol.* **1998**, *2*, 24–30.

32 Rupert, P. B.; Massey, A. P.; Sigurdsson, S. T.; Ferré-D'Amaré, A. R. *Science* **2002**, *298*, 1421–1424.

33 Herschlag, D.; Piccirilli, J. A.; Cech, T. R. *Biochemistry* **1991**, *30*, 4844–4854.

34 Usman, N.; Cedergren, R. *Trends Biochem. Sci.* **1992**, *17*, 334–339.

35 Catrina, I. E.; Hengge, A. C. *J. Am. Chem. Soc.* **1999**, *121*, 2156–2163.

36 Puerta-Fernández, E.; Romero-López, C.; Barroso-delJesus, A.; Berzal-Herranz, A. *FEMS Microbiol. Rev.* **2003**, *27*, 75–97.

37 Smith, J. S.; Nikonowicz, E. P. *Biochemistry* **2000**, *39*, 5642–5652.

38 Catrina, I. E.; Hengge, A. C. *J. Am. Chem. Soc.* **2003**, *125*, 7546–7552.

39 Zhou, D.-M.; Taira, K. *Chem. Rev.* **1998**, *98*, 991–1026.

40 Breslow, R.; Chapman, Jr., W. H. *Proc. Natl. Acad. Sci. USA* **1996**, *93*, 10018–10021.

41 Åqvist, J.; Kolmodin, K.; Florian, J.; Warshel, A. *Chem. Biol.* **1999**, *6*, R71–R80.

42 Karplus, M. *J. Phys. Chem. B* **2000**, *104*, 11–27.

43 Friesner, R. A.; Beachy, M. D. *Curr. Opin. Struct. Biol.* **1998**, *8*, 257–262.

44 Warshel, A. *Annu. Rev. Biophys. Biomol. Struct.* **2003**, *32*, 425–443.

45 Yun Liu, X. L.; York, D. M. *Chem. Comm., submitted*.

46 Almer, H.; Strömberg, R. *Tetrahedron Lett.* **1991**, *32*, 3723–3726.

47 Oivanen, M.; Kuusela, S.; Lönnberg, H. *Chem. Rev.* **1998**, *98*, 961–990.

48 Ora, M.; Järvi, J.; Oivanen, M.; Lönnberg, H. *J. Org. Chem.* **2000**, *65*, 2651–2657.

49 Liu, X.; Reese, C. B. *Tetrahedron Lett.* **1996**, *37*, 925–928.

50 Weinstein, L. B.; Earnshaw, D. J.; Cosstick, R.; Cech, T. R. *J. Am. Chem. Soc.* **1996**, *118*, 10341–10350.

51 Dantzman, C. L.; Kiessling, L. L. *J. Am. Chem. Soc.* **1996**, *118*, 11715–11719.

52 Silva, C. O.; da Silva, E. C.; Nascimento, M. A. C. *J. Phys. Chem. A* **2000**, *104*, 2402–2409.

53 Lide, D. R., *edt. CRC handbook of chemistry and physics*. CRC Press LLC, Boca Raton, FL, 83 edition, **2003**.

54 Perreault, D. M.; Anslyn, E. V. *Angew. Chem. Int. Ed.* **1997**, *36*, 432–450.

55 Liu, X.; Reese, C. B. *Tetrahedron Lett.* **1995**, *36*, 3413–3416.

56 Thomson, J. B.; Patel, B. K.; Jiménez, V.; Eckart, K.; Eckstein, F. *J. Org. Chem.* **1996**, *61*, 6273–6281.

57 Warshel, A.; Levitt, M. *J. Mol. Biol.* **1976**, *103*, 227–249.

58 Åqvist, J.; Warshel, A. *Chem. Rev.* **1993**, *93*, 2523–2544.

59 Gao, J. *Rev. Comput. Chem.* **1995**, *7*, 119–185.

60 Gao, J.; Truhlar, D. G. *Annu. Rev. Phys. Chem.* **2002**, *53*, 467–505.

61 Gregersen, B. A.; Lopez, X.; York, D. M. *J. Am. Chem. Soc.* **2004**, *126*, 7504–7513.

62 Rashin, A. A. *J. Phys. Chem.* **1990**, *94*, 1725–1733.

63 Cramer, C. J.; Truhlar, D. G. *Chem. Rev.* **1999**, *99*, 2161–2200.

64 Thiel, W.; Voityuk, A. A. *Theor. Chim. Acta* **1992**, *81*, 391–404.

65 Riccardi, D.; Li, G.; Cui, Q. *J. Phys. Chem. B* **2004**, *108*, 6467–6478.

66 Gao, J.; Xia, X. *Science* **1992**, *258*, 631.

67 York, D. M.; Lee, T.-S.; Yang, W. *J. Am. Chem. Soc.* **1996**, *118*, 10940–10941.

68 Garcia-Viloca, M.; Truhlar, D. G.; Gao, J. *J. Mol. Biol.* **2003**, *327*, 549–560.

69 Garcia-Viloca, M.; Gao, J.; Karplus, M.; Truhlar, D. G. *Science* **2004**, *303*, 186–195.

70 Bader, J. S.; Chandler, D. *J. Phys. Chem.* **1992**, *96*, 6423–6427.

71 Gregersen, B. A.; York, D. M. *J. Phys. Chem. B* **2005**, *109*, 536–556.

72 Jackson, J. D. *Classical electrodynamics*. Wiley, New York, 3 edition, 1999.